Comparative Visualization of Orientation Tensors in Fiber-Reinforced Polymers

Johannes Weissenböck[1], Mustafa Arikan[1], Dietmar Salaberger[1], Johann Kastner[1], Jan De Beenhouwer[2], Jan Sijbers[2], Stefanie Rauchenzauner[3], Tanja Raab-Wernig[4], Eduard Gröller[5], Christoph Heinzl[1]

[1]University of Applied Sciences Upper Austria - Wels Campus, Stelzhamerstraße 23, Wels, Austria, e-mail: johannes.weissenboeck@fh-wels.at, mustafa.arikan@fh-wels.at, dietmar.salaberger@fh-wels.at, johann.kastner@fh-wels.at, christoph.heinzl@fh-wels.at

[2]imec-VisionLab, University of Antwerp, Universiteitsplein 1, Antwerp, Belgium, e-mail: jan.debeenhouwer@uantwerpen.be, jan.sijbers@uantwerpen.be

[3]FACC Operations GmbH, Fischerstraße 9, Ried im Innkreis, Austria, e-mail: s.rauchenzauner@facc.com

[4]ZKW Group GmbH, Rottenhauser Straße 8, Wieselburg an der Erlauf, Austria, e-mail: tanja.raab-wernig@zkw.at

[5]TU Wien and VrVis Research Center, Vienna, Austria, e-mail: groeller@cg.tuwien.ac.at

More info about this article: http://www.ndt.net/?id=21912

Abstract

Industrial 3D X-ray computed tomography (XCT) has been adopted in the industries as a high-resolution non-destructive testing method. XCT enables resolving individual fibers, which is the basis for calculating the fiber orientation of each individual fiber and fiber orientation tensors, respectively. In this work, we present an interactive visualization tool for comparing the orientation tensor information between simulation and real-world XCT data or between two real-world XCT data. Based on the orientation tensor data we calculate three different similarity measures (degree of orientation, cosine similarity and tensor similarity) to characterize the data. The calculated measures are presented with heat maps to show the fiber orientation correlations between simulation and real-world XCT data. In addition, we use superquadric tensor glyphs to visualize and compare the fiber orientations of the simulation data and the XCT data. This type of glyphs, introduced by Kindlmann et. al., convey tensor variables by mapping the tensor eigenvectors and eigenvalues to the orientation and shape of a geometric primitive. The superquadric tensor glyphs and the heat maps of the similarity measures are shown layer by layer and can be overlaid onto each other. We demonstrate our tool by using an injection molded short glass fiber-reinforced polymer specimen.

Keywords: X-ray computed tomography, simulation, fiber-reinforced polymers, tensor, visualization, glyphs

1 Introduction and Motivation

Short-fiber-reinforced polymer (SFRP) materials are frequently used in the automotive, aeronautic, and leisure industry. The fibers improve the physical properties of the matrix material and allow enhancing the mechanical properties, high throughput, as well as cost reductions [1]. SFRP components are often manufactured by means of injection molding [2–3]. During the injection molding process, the base materials (e.g., polymeric matrix and glass fibers) are heated, mixed, and subsequently forced into the mold with pressure. Afterwards, the SFRP component is cured in a cooling phase. During the injection molding process, unwanted local flow-induced fiber misalignments are created which have a bad influence on the final material properties (e.g. stiffness and strength). These properties mainly depend on the orientation of the individual fibers [1] which makes the analysis of fiber orientations an important task for prototyping and quality assurance. To check the result of the molding process, it is important for the domain experts to compare and validate the FRP materials with each other or with a reference specimen.

The simulation of the injection molding process is part of the optimization of the manufacturing process. The main goal of the simulation is to predict the flow-induced orientation of fibers. The simulation implements a model, which mimics the molding machinery, e.g., the mold and the process conditions to control the desired fiber orientations [1]. The simulation requires parameters such as pressure, temperature, and cooling. Improper setting of the parameters may result in differences between the simulation and the final product. The simulation runs are cheap and fast, but suffer from the varying accuracy of the models (especially for complex structures). Therefore, the simulation model needs to be carefully validated.

A commonly used approach to determine the individual fiber orientations is the optical microscopy [4]. This method has the drawback that it is expensive, destructive, and only provides 2D or 2.5D information on the fiber orientations.

The industrial 3D X-ray computed tomography (XCT) on the other hand, has excelled as a high-resolution non-destructive testing method in recent years. Because of the high resolution of the currently available XCT systems, the individual fibers in the SFRP specimen can be resolved and the corresponding fiber orientations can be calculated [5–7].

Due to the close collaboration with the material experts, we were able to abstract the domain-specific requirements and identified the following tasks for the comparative visualization of simulation data and XCT data (or XCT data versus XCT data) in SFRP materials:

- **Task 1: Visualization of orientation strength.**
  The strength of the orientation provides information on how many fibers are oriented in the same direction.
- **Task 2: Visualization of direction strength.**
  The strength of the direction indicates the main orientation of the fibers.
- **Task 3: Visualization of similar regions.**
  For the experts, it is important to identify regions where the simulation and the XCT tensors are similar.

To address the tasks identified by the domain experts, we introduce a novel tool to visually explore, analyze and compare the fiber orientations of injection molding SFRP materials. The tool allows comparing a simulation and an XCT scan or two XCT scans against each other. In the following work we demonstrate our tool based on a simulation and an XCT scan of a real-world SFRP injection molding specimen.

The work flow (see Figure 1) starts with a high-resolution XCT scan of the specimen and the import of the simulation data into our tool. In a preprocessing step the individual fibers are segmented and characteristics, e.g. fiber starting and ending point and fiber orientation, are calculated. Based on the fiber characteristics, the XCT dataset is subdivided into cells. For each cell an orientation tensor is calculated. The software solution used by our collaborators for the simulation generates the orientation tensors which describe the fiber orientations. To compare the simulation data with the XCT dataset, the simulation data need to be correctly registered to the Cartesian grid of the XCT dataset and the orientation tensors of the simulation data need to be rotated in to the coordinate system of the XCT dataset. Superquadric tensor glyphs and heat maps are used to compare the fiber orientation information of the simulation data and the XCT dataset (or two XCT datasets) to find similar regions.

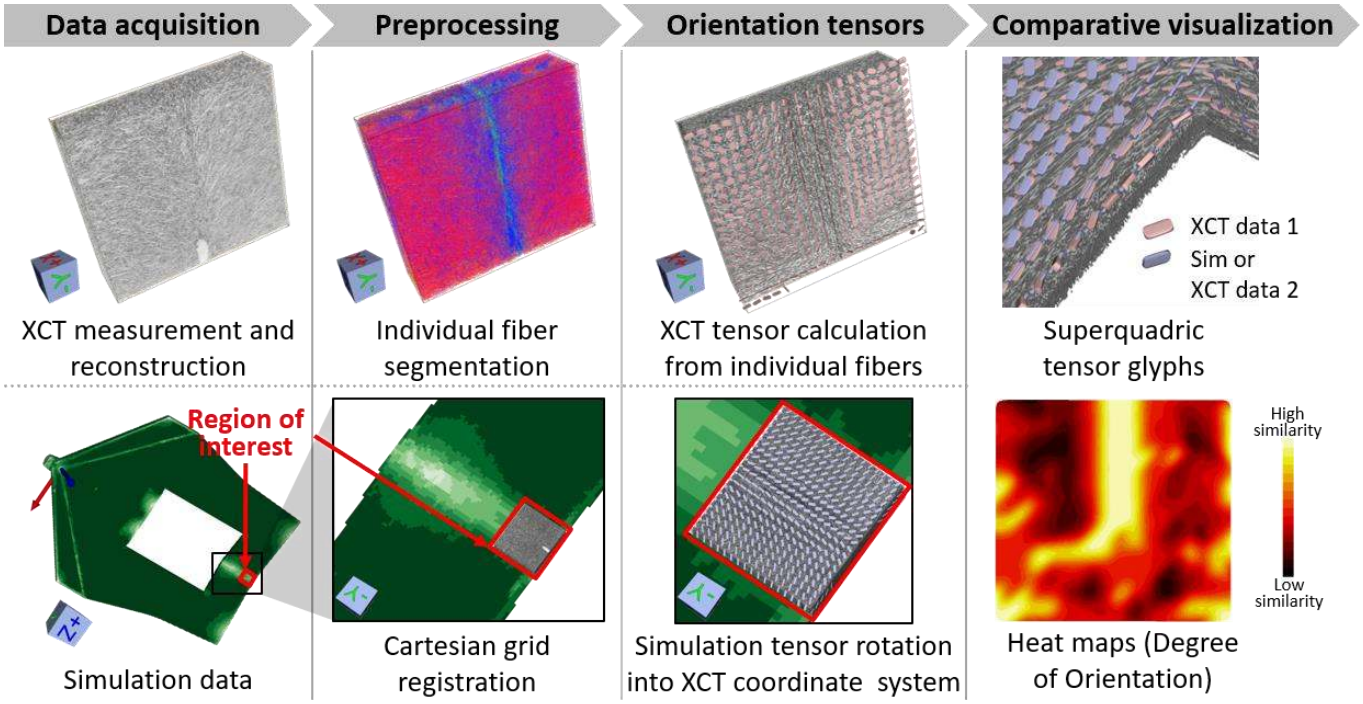

Figure 1: The comparative visualization pipeline for the interactive exploration and visual analysis of fiber orientations in SFRPs between simulation and real-world XCT scans consists of four stages: data acquisition, preprocessing, calculation of orientation tensors and comparative visualization.

2 Related Work

Visualizations of fiber orientations are typically accomplished by rendering lines or arrows corresponding to each individual fiber and its orientation [8]. Using spherical color maps as presented by Yamrom et al. [9] the orientations of the individual fibers may be color-coded in the 3D domain. However, due to the large number of fibers even in a small cutout of an SFRP component, which may exceed thousands of fibers, domain users are confronted with information overload and visual clutter. In a more recent work by Weissenböck et al. [10, 43], interactive tools for exploring and analyzing fiber-reinforced polymers were presented. Amirkhanov et. al. presented a framework to visually analyze defects in glass fiber-reinforced polymers for 4DCT interrupted in situ tests [44]. Sedlmair et. al. introduced an abstract conceptual framework to describe, discuss, and evaluate visual parameter space analysis solutions across different application domains [45]. Heinzl et. al. presented a systematic survey on the close interrelations between visual computing and materials science [46].
In the following sections we review the state of the art in second-order tensor visualization as well as comparative visualization.

2.1 Visualization of Second-Order Tensors

In the field of diffusion tensor imaging (DTI), there is much research focusing on the visualization of second order tensors [11–13] or fiber tracking [14–17]. The goal of DTI is to visualize microstructures of the brain by measuring the local diffusion of water molecules in the tissue. Streamlines and hyper-streamlines continuously show directional information in the volume [11, 18–20]. The disadvantages of hyper-streamlines however are clutter and occlusion. We opted for using glyphs as a comparative visualization to describe similarities and differences in local regions. Pierpaoli et al. [13] use ellipsoidal glyphs for the visualization of DTI data. Laidlaw et al. [12] use normalized ellipsoids at each pixel to provide a simple interpretation of a DTI image. Chen et al. [21] are combining ideas from integral curves and ellipsoids to visualize connectivity information while characterizing the local tensors in detail. Neeman et al. [22] and Hotz et al. [23] present visualization methods for stress and strain tensors from geomechanics. Auer et al. [24] reviewed the visualization methods of texture mapping and glyph placement designed for tensor fields arising in applications such as physics and mechanical engineering. Kindlmann [25] introduced superquadric tensor glyphs to address the problems of asymmetry and ambiguity of cuboids and ellipsoids in visualization. Westin [26] visualizes second-order tensors using a spear, a plate, and a sphere for better interpretation. Bergmann et al. [27] introduced a multi-tensor model to estimate several diffusion tensors per voxel for a DTI dataset. While the above-mentioned approaches can handle visualizations of tensors and tensor fields, they do not address the visual comparison of tensor fields.

2.2 Comparative Visualization

The work of Gleicher et al. [28] describes the three basic concepts of comparative visualization: juxtaposition, superposition, and explicit encoding of relationships. Hlawatsch et al. [29] introduced a method to separate the domain of a tensor field into qualitatively different regions and to further structure regions perceived as coherent. Malik et al. [30] present a novel multi-image view and an edge explorer for simultaneously comparing and visualizing gray values and edges of several datasets with varying scan parameters. Schmidt et al. [31] proposed a new comparative visualization approach for detailed analysis of large image datasets. Hummel et al. [32] introduced an approach for comparison of sets of simulation runs based on parameter and model variation to classify and identify common and contradictory trends in Lagrangian flows. Peeters et al. [33] explain several distance and similarity measures for diffusion tensors.

3 Domain Background

3.1 Fiber Orientation

The visualization of individual fibers could be accomplished by rendering simple lines or arrows. But due to the high number of fibers, which typically exceeds hundreds of thousands of fibers, one is confronted with information overload. The orientation of a single fiber is presented in Figure 2 [1, 34]:

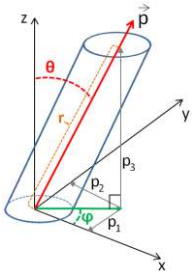

Figure 2: The vector $\vec{p}$ represents a single fiber with (p1, p2, p3) in the Cartesian coordinate system. A second representation is defined by $(r = 1, \theta, \phi)$ in a spherical coordinate system.

$$p_1 = \sin\theta \cos\varphi \tag{1}$$

$$p_2 = \sin\theta \sin\varphi \tag{2}$$

$$p_3 = \cos\theta \tag{3}$$

The equations (1), (2), and (3) are used for the conversion between the Cartesian coordinate system and the spherical coordinate system.

3.2 Orientation Tensor

Orientation tensors are symmetric second-order tensors calculated as the dyadic product of the unit vectors $\vec{p}$. Orientation tensors represent an average orientation calculated from the individual fibers [34]. The orientation tensor T is given as:

$$T = \begin{pmatrix} a_{11} & a_{12} & a_{13} \\ . & a_{22} & a_{23} \\ . & . & a_{33} \end{pmatrix} = \begin{pmatrix} {p_1}^2 & p_1p_2 & p_1p_3 \\ p_1p_2 & {p_2}^2 & p_2p_3 \\ p_1p_3 & p_2p_3 & {p_3}^2 \end{pmatrix} \tag{4}$$

For a group of n individual fibers the average orientation tensor is calculated using the following formula, where i and j refer to the indices of the tensor and k to the kth fiber within a region [35]:

$$a_{avg_{ij}} = \frac{1}{n}\sum_{k=1}^{n} {a_{ij}}^k \tag{5}$$

3.3 Degree of Orientation

The degree of orientation O_D is a scalar value to describe the strength of the main orientation of a tensor. It is calculated by normalizing the largest eigenvalue. The sum of the diagonal entries equals 1. The diagonal tensor elements lie between 0 and 1.

$$a_{11} + a_{22} + a_{33} = 1 \quad \text{and} \quad 0 < a_{ii} < 1 \quad \text{with} \quad 0 < i \leq 3 \tag{6}$$

The lowest value for the largest eigenvalue is $\frac{1}{3}$, since the sum of all three eigenvalues is 1. We normalize the degree of orientation to get values between 0 and 1. The degree of orientation is O_D. The largest eigenvalue is represented by λ_1:

$$O_D = \frac{3}{2}\left(\lambda_1 - \frac{1}{3}\right) \tag{7}$$

3.4 Cosine Similarity

The cosine similarity allows comparing the main direction of the fiber orientations. We calculate the angle α between these two vectors ($\mathrm{Vec}_{\mathrm{Dataset\ 1}}$ and $\mathrm{Vec}_{\mathrm{Dataset\ 2}}$) using the dot product. The two vectors are similar if the value for the cosine similarity $\mathrm{Similarity}_{\mathrm{C}}$ is 1. Two vectors are different if the value for the cosine similarity is -1. Because of the symmetry of the fiber orientations the value for the difference should be between 0 (90°) and 1 (0°). To limit the range between 0 and 1 we calculate the absolute value for the cosine similarity.

$$Similarity_C = |\cos\alpha| = |Vec_{Dataset\ 1} \times Vec_{Dataset\ 2}| \tag{8}$$

3.5 Tensor Similarity

In the sections above, we compare partial information of the tensor. The degree of orientation relates only to the largest eigenvalue. The cosine similarity relates to the eigenvector of the largest eigenvalue. To compare the whole information of the tensor we can use the following formula to calculate the tensor similarity $\mathrm{Similarity}_{\mathrm{T}}$ [36–37]:

$$Similarity_T = \sqrt[2]{\sum_{i=1}^{3}\sum_{j=1}^{3}\left(a_{ij} - b_{ij}\right)^2} \tag{9}$$

4. Data Acquisition and Preprocessing

4.1 Dataset Description

The specimen is a polypropylene based composite reinforced with short glass fibers. The dimensions are 210x4x170 mm. The simulation software Moldflow Insight™ was used to model the specimen. The XCT scanned dataset, shown in Figure 4(b), is 1770x520x1909 voxels in size with a resolution of 5 µm. The specimen is scanned with a GE phoenix|X-Ray Nanotom 180.

4.2 Individual Fiber Segmentation

A considerable amount of literature has been published on Hessian-based segmentation of tubular structures from medical images [38]. However, there are some drawbacks when applying Hessian-based segmentation or enhancement filters on XCT data of polymer composites with fibers. Because of the high fiber content, many fibers are intersecting or touching each other which makes the segmentation of the individual fibers difficult and leads to problems like virtual fiber breakage, false fiber connection, and multi fiber merging (into one fiber) [39]. To overcome these problems and to improve the individual fiber segmentation, we propose a template matching approach [40]. We exploit the uniformity of fiber diameters and use a sphere as a template. The diameter of the template sphere corresponds to the mean diameter of the fibers. The fiber extraction is described in Figure 3.

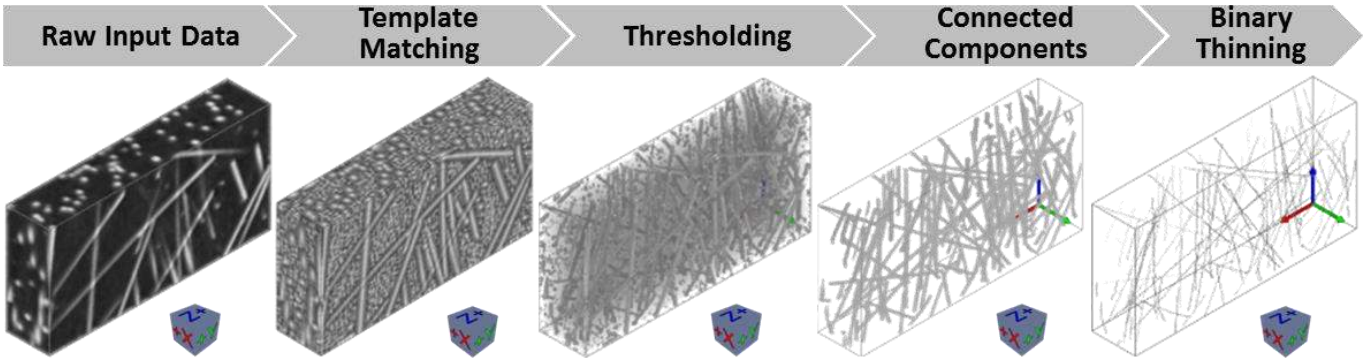

Figure 3: The following steps are applied to the raw input data to segment the individual fibers: extraction of the medial fiber axis using the template matching approach, thresholding to separate the fibers from the polymer matrix, connected component filtering, and binary thinning to calculate the characteristics of individual fibers from their centerlines.

In a first step the medial axes of the fibers are determined using the template matching approach. For this approach we calculate a normalized correlation coefficient at each voxel of the input image. A threshold is applied to separate the fibers from the polymer matrix. In the next step we use a connected component filter and count the number of voxels for every region. If the number of the voxels for a region is below a user-defined threshold we remove that region. This is done to avoid the segmentation of noise and short fiber particles, which are not considered as fibers. After this, we use a binary thinning filter to get fibers with one-voxel wide centerlines and assign a unique label to every fiber. In a post-processing step, we use the centerlines with unique labels to calculate fiber lengths and fiber orientations.

4.3 Orientation Tensors Computation

The orientation tensor for a cell (of the XCT dataset) is computed by first computing the orientation tensors for the individual fibers which belong to the particular cell, and averaging them. The first step involves getting the starting and ending point of the fiber. After that, we subtract one point from each another. The result is a vector defined by {dX, dY, dZ}. Then we translate this vector to the origin. The result is a line defined by the origin (0, 0, 0) and the position (p1, p2, p3). For the calculation of the orientation tensor (see Equation (4)), we then transform the position from the Cartesian coordinate system to the spherical coordinate system:

$$Define\ zAxis\ with\ \{0,0,1\} \tag{10}$$

$$Define\ vector\ with\ \{p1,p2,p3\} \tag{11}$$

$$\theta = arcos\frac{p3}{\|\overrightarrow{zAxis}\|\|\overrightarrow{vector}\|} \tag{12}$$

$$Define\ xAxis\ on\ xy\ plane\ with\ \{1,0\ ,0\} \tag{13}$$

$$Define\ vector2\ with\ p1,p2 \tag{14}$$

$$\varphi = arcos\frac{p1}{\|\overrightarrow{xAxis}\|\|\overrightarrow{vector2}\|} \tag{15}$$

4.4 Registration of Simulation Data

The simulation software (Moldflow InsightTM) generates a dataset which consists of an unstructured grid with the geometry of the real specimen. The simulated dataset is separated into several layers. Each layer contains several hexahedral cells. The output contains a single orientation tensor per cell. The hexahedral cells are defined by eight grid points. The points of the simulation grid are specified in the Cartesian coordinate system. In a registration step the simulation and the XCT data are overlaid onto each other. This allows us to define the regions for the computation of the orientation tensors from the XCT data. We set up a transformation matrix from the simulation's coordinate system to the XCT dataset's coordinate system. For the rotation, we defined the matrix Q [41]:

$$Q = \begin{pmatrix} u^2(1-\cos\alpha)+\cos\alpha & uv(1-\cos\alpha)-w\sin\alpha & uw(1-\cos\alpha)-v\sin\alpha \\ uv(1-\cos\alpha)+w\sin\alpha & v^2(1-\cos\alpha)+\cos\alpha & vw(1-\cos\alpha)+u\sin\alpha \\ uw(1-\cos\alpha)-v\sin\alpha & vw(1-\cos\alpha)+u\sin\alpha & w^2(1-\cos\alpha)+\cos\alpha \end{pmatrix} \tag{16}$$

We apply Q according to Equation (17) on all grid points. The vector defined by {u, v, w} could be any arbitrary unit vector, for example, {1, 0, 0} for a rotation around the x-axis. And α is the rotation angle [42].

$$\overrightarrow{P_R} = Q\vec{P} \tag{17}$$

$\vec{P}$ represents a grid point with coordinates (x, y, z). And $\overrightarrow{P_R}$ is the result of the rotation. The rotation of a tensor from one coordinate system to another follows Equation (18), where T_R is the rotated tensor (in the coordinate system of the XCT volume) and the T is the original tensor (in the coordinate system of the simulation):

$$T_R = Q\ T\ Q^T \tag{18}$$

5. Comparative Visualization Results

5.1 Superquadric Tensor Glyphs

The information of the orientation tensors (e.g., from XCT data and simulation data) are used to generate the superquadric tensor glyphs. As described in Section 4.3, one glyph is calculated for one cell. Figure 4(a) shows the simulated SFRP injection molding dataset with the color-coded degree of orientation for layer 2. White means a varying orientation of the fibers, dark-green means a uniform orientation. A region at the end of the injection molding part has been scanned via XCT. The XCT dataset is registered to the simulation data (red rectangle). A detailed view of the XCT dataset is presented in Figure 4(b), which shows the individual fibers. Figure 4(c) depicts the superquadric tensor glyphs. The blue colored glyphs represent the orientation tensors of the simulation data; the cyan colored glyphs represent the orientation tensors of the XCT scan. Especially the yellow marked areas show correlation of the fiber orientations between the simulation data and the real-world XCT data.

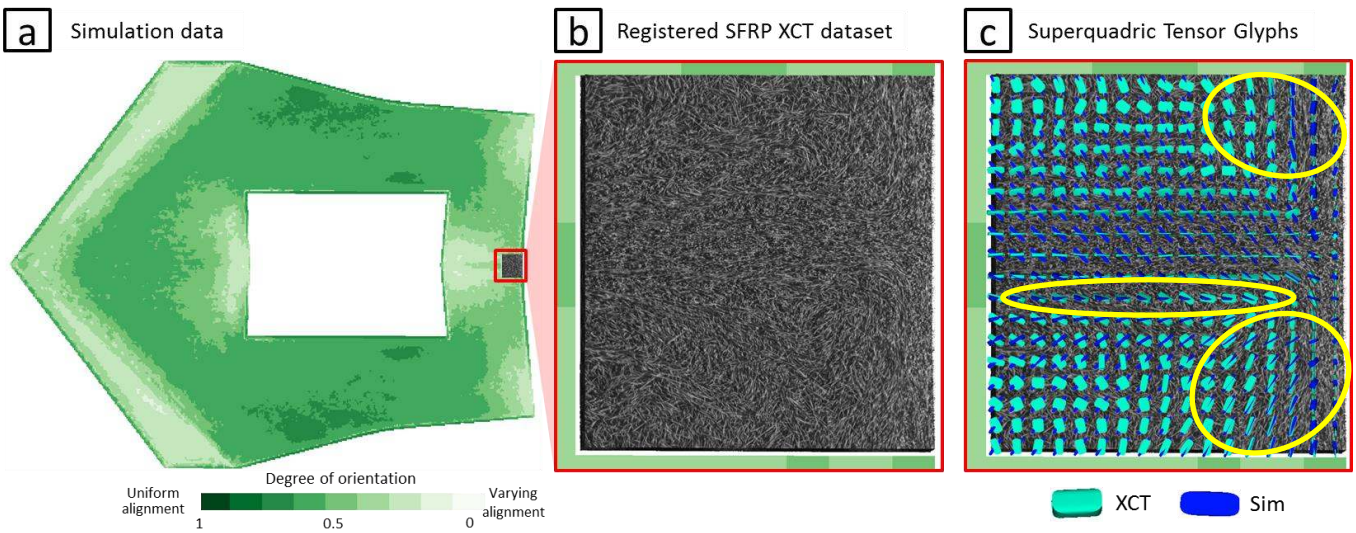

Figure 4: (a) shows the simulation data of the SFRP injection molding part (layer 2) with the color-coded degree of orientation. (b) presents a detailed view of the registered XCT scan. (c) the overlaid superquadric tensor glyphs (simulation: blue, XCT: cyan). The yellow areas mark regions with uniform correlations of the fiber orientations between simulation and XCT.

5.2 Degree of Orientation

As described in Section 3.3, the degree of orientation represents the strength of the main orientation of a tensor. The degree of orientation is color-coded with a sequential color map ranging from white (varying alignment of the fibers) to dark-green (uniform alignment of the fibers). Figure 5(a) shows the simulation data with the registered SFRP XCT dataset (red rectangle) for layer 2. Figure 5(b) shows the encoded degree of orientation information of the XCT scan. The yellow areas mark regions with a high degree of orientation (fibers with uniform alignment).

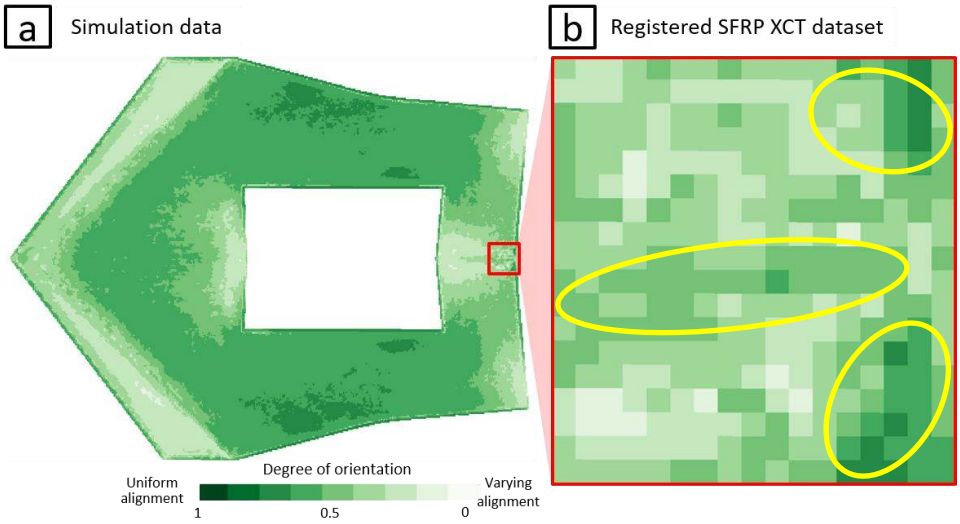

Figure 5: (a) shows the simulation data of the SFRP injection molding part (layer 2) with the color-coded degree of orientation and (b) the detailed view of the registered SFRP XCT dataset with yellow marked areas which represent high degree of orientation (fibers with uniform alignment).

5.3 Cosine Similarity

The cosine similarity allows comparing the main direction of the fiber orientations between the simulation data the XCT data (see Section 3.4). Figure 6(a) shows the simulation data with the registered SFRP XCT dataset (red rectangle) for layer 2. Figure 6(b) depicts a detailed view of the registered SFRP XCT dataset by showing the cosine similarity as a heat map. Black areas represent a low similarity and yellow areas represent a high similarity between the simulation data and the XCT data. Figure 6(c) presents the cosine similarity heat map with the overlaid superquadric tensor glyphs. Due to the heat map, regions with similar orientations can be easily perceived.

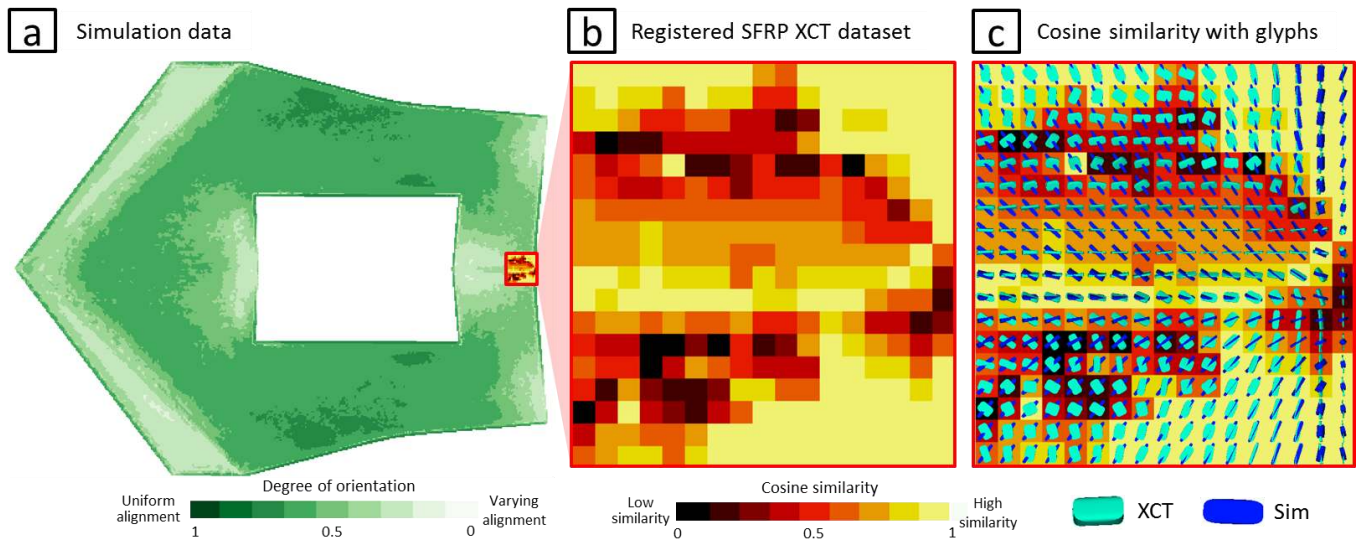

Figure 6: (a) shows the simulation data of the SFRP injection molding part (layer 2) with the color-coded degree of orientation and (b) the detailed view of the registered SFRP XCT dataset with the color-coded cosine similarity (black: low similarity, yellow: high similarity). (c) presents the color-coded cosine similarity and with the overlaid superquadric tensor glyphs.

5.4 Tensor Similarity

As discussed in Section 3.5, the tensor similarity enables comparing the whole tensor information (in contrast to the cosine similarity). Figure 6(a) shows the simulation data with the registered SFRP XCT dataset (red rectangle) for layer 2. Figure 7(b) depicts a detailed view of the registered SFRP XCT dataset by showing the tensor similarity as a heat map. Black areas represent a low similarity and yellow areas represent a high similarity between the simulation data and the XCT data. In comparison to the cosine similarity, the tensor similarity is less conservative and shows more similar regions, as it only generates values above 0.3 (in this cutout). Figure 7(c) presents the tensor similarity heat map with the overlaid superquadric tensor glyphs. Due to the heat map, the similar regions can be clearly identified.

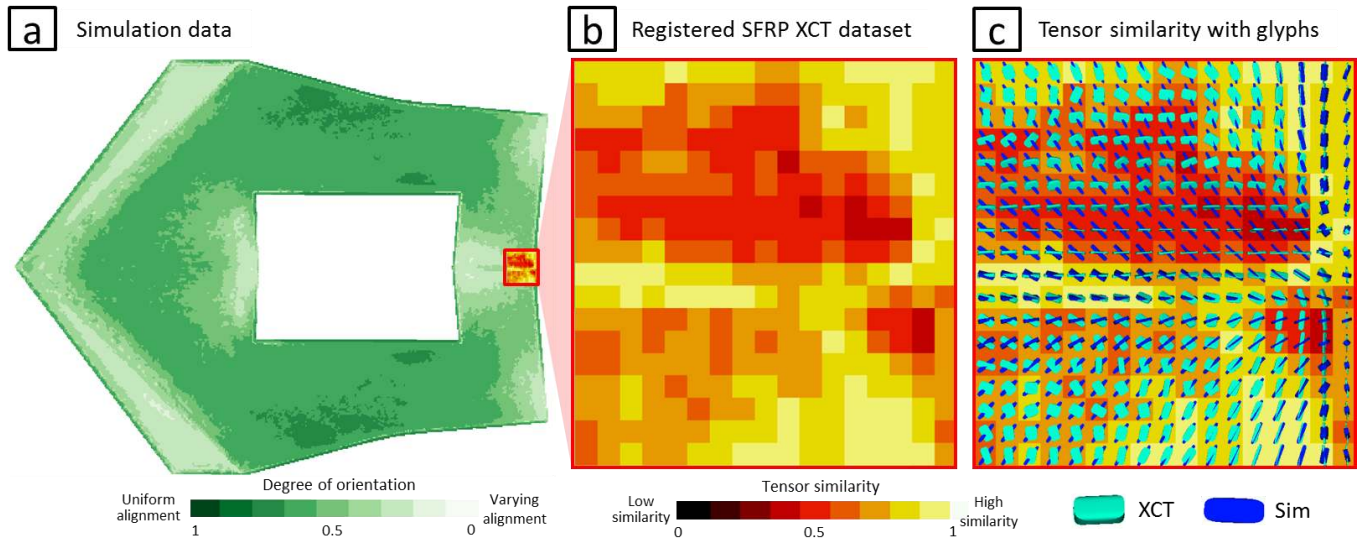

Figure 7: (a) shows the simulation data of the SFRP injection molding part (layer 2) with the color-coded degree of orientation and (b) the detailed view of the registered SFRP XCT dataset with the color-coded tensor similarity (black: low similarity, yellow: high similarity). (c) presents the color-coded tensor similarity and with the overlaid superquadric tensor glyphs.

6. Conclusion

We presented a tool to visually explore, analyze and compare the fiber orientations between the simulation data and the XCT data of an injection molding SFRP specimen. The tool also allows comparing the fiber orientations of two XCT datasets. We showed several measures, e.g., degree of orientations, cosine similarity, and tensor similarity which serve as input for the superquadric tensor glyphs and the color-coded heat map. By using these comparative visualization concepts, regions with similar fiber orientations are highlighted to increase the perception of these interesting areas. Furthermore, we demonstrated that our tool helps to bridge the gap between simulation and the industrial process of injection molding. We have shown an

approach for the validation of simulation data and XCT data. It has the potential to improve the workflow of the domain experts in plastics industry.

Acknowledgements

The research leading to these results has received funding from the FFG Bridge Early Stage project no. 851249: Advanced multimodal data analysis and visualization of composites based on grating interferometer micro-CT data (ADAM), as well as the Research Foundation Flanders (FWO) and the Austrian Science Fund (FWF) under the grant numbers G0F9117N and I3261-N36 respectively: Quantitative X-ray tomography of advanced polymer composites.

References

[1] G.M. Vélez-García, Experimental evaluation and simulations of fiber orientation in injection molding of polymers containing short glass fibers, Virginia Polytechnic Institute and State University, 2012.
[2] Z. Gombos, Analysis of glass fiber mat structures and their impact on the resin absorption process and on the characteristics of composites, PhD thesis, Budapest University of Technology and Economics, 2010.
[3] S. Thomas, K. Joseph, S. Malhotra, K. Goda, S. Sreekala, Polymer Composites, Macro- and Microcomposites, Polymer Composites, Wiley, 2012.
[4] P. Hine, N. Davidson, R. Duckett, I. Ward, Measuring the fibre orientation and modelling the elastic properties of injection-moulded long-glass-fibre-reinforced nylon. Composites Science and Technology 53(2): 125 – 131, 1995.
[5] A. Bernasconi, F. Cosmi, P. J. Hine, Analysis of fibre orientation distribution in short fibre reinforced polymers: A comparison between optical and tomographic methods, Comp. Sci. and Technology, 72(16): 2002–2008, 2012.
[6] T. B. Nguyen Thi, M. Morioka, A. Yokoyama, S. Hamanaka, K. Yamashita, C. Nonomura, Measurement of fiber orientation distribution in injection-molded short-glass-fiber composites using X-ray computed tomography, Journal of Materials Processing Technology, 219: 1–9, 2015.
[7] D. Tsarouchas, A.E. Markaki, Extraction of fibre network architecture by X-ray tomography and prediction of elastic properties using an affine analytical model, Acta Materialia, 59(18): 6989–7002, 2011.
[8] D. Salaberger, K. Kannappan, J. Kastner, J. Reussner, T. Auinger, CT Data evaluation of fibre reinforced polymers to determine fibre length distribution, International Polymer Processing, 3: 283-291, 2011.
[9] B. Yamrom, J. A. Sutliff, A. P. Woodfield, .: Visualizing polycrystalline orientation microstructures with spherical color maps. In Proceedings of the IEEE conference on Visualization, 1994.
[10] J. Weissenböck, A. Amirkhanov, W. Li, A. Reh, A. Amirkhanov , E. Gröller, J. Kastner, C. Heinzl, Fiberscout: An interactive tool for exploring and analyzing fiber reinforced polymers. IEEE Pacific Vis. Symp., pages 153–160, 2014.
[11] F. Enders, N. Sauber, D. Merhof, P. Hastreiter, C. Nimsky, and M. Stamminger, Visualization of white matter tracts with wrapped streamlines. In Proceedings of the IEEE conference on Visualization, pages 51–58, 2005.
[12] D. Laidlaw, E. Ahrens, D. Kremers, M. Avalos, R. Jacobs, and C. Readhead. Visualizing diffusion tensor images of the mouse spinal cord. In Proceedings of the IEEE conference on Visualization, pages 127–134, 1998.
[13] C. Pierpaoli and P. J. Basser. Toward a quantitative assessment of diffusion anisotropy. Magnetic Resonance in Medicine, 26:893–906, 1996.
[14] R. Brecheisen, A. Vilanova, B. Platel, and B. ter Haar Romeny. Parameter sensitivity visualization for DTI fiber tracking. IEEE Transactions on Visualization and Computer Graphics, 15(6):1441–1448, 2009.
[15] W. Chen, Z. Ding, S. Zhang, A. MacKay-Brandt, S. Correia, H. Qu, J. A. Crow, D. F. Tate, Z. Yan, and Q. Peng. A novel interface for interactive exploration of dti fibers. IEEE Trans. Vis. Comput. Graphics, 15(6):1433–1440, 2009.
[16] B. Moberts, A. Vilanova, and J. van Wijk. Evaluation of fiber clustering methods for diffusion tensor imaging. In Proceedings of the IEEE conference on Visualization, pages 65–72, 2005.
[17] P. Svetachov, M. H. Everts, T. Isenberg, DTI in context: Illustrating brain fiber tracts in situ. Computer Graphics Forum 29, 3, 1023–1032, 2010.
[18] G. Kindlmann, D. Weinstein, and D. Hart, Strategies for direct volume rendering of diffusion tensor fields, IEEE Transactions on Visualization and Computer Graphics, 6(2):124–138, 2000.
[19] B. Spencer, R. S. Laramee, G. Chen, and E. Zhang, Evenly spaced streamlines for surfaces: An image-based approach, Computer Graphics Forum, 28(6):1618–1631, 2009.
[20] D. Zhang, Smith, Jack, and S. Montgomery-Smith, Numerical Evaluation of Single Fiber Motion for Short-Fiber-Reinforced Composite Materials Processing, J. of Manuf. Sci. Eng., 133(5):051002-051002-9, 2011.
[21] W. Chen, S. Zhang, S. Correia, and D. Tate, Visualizing diffusion tensor imaging data with merging ellipsoids, In IEEE Pacific Visualization Symposium, pages 145–151, 2009.
[22] A. Neeman, B. Jeremic, and A. Pang, Visualizing tensor fields in geomechanics, IEEE Visualization, pp. 35–42, 2005.
[23] I. Hotz, L. Feng, H. Hagen, B. Hamann, K. Joy, and B. Jeremic, Physically based methods for tensor field visualization, In IEEE Visualization, pages 123–130, 2004.
[24] C. Auer, C. Stripf, A. Kratz, and I, Hotz, Glyph- and texture-based visualization of segmented tensor fields, In GRAPP/IVAPP, pages 670–677, 2012.
[25] G. L. Kindlmann, Superquadric tensor glyphs, IEEE TCVG Conference on Visualization, pages 147–154, 2004.
[26] C.-F. Westin, A Tensor Framework for Multidimensional Signal Processing, PhD thesis, Linköping University, 1994.

[27] Ø. Bergmann, G. Kindlmann, A. Lundervold, and C.-F. Westin, Diffusion k-tensor estimation from q-ball imaging using discretized principal axes, Intern. Conf. Med. Image Comp. and Comp.-Ass. Interv. (MICCAI'06), pp. 268–275, 2006.
[28] M. Gleicher, D. Albers, R. Walker, I. Jusufi, C. D. Hansen, and J. C, Roberts, Visual comparison for information visualization, Information Visualization, 10(4):289–309, 2011.
[29] M. Hlawatsch, J. E. Vollrath, F. Sadlo, and D. Weiskopf, Coherent structures of characteristic curves in symmetric second order tensor fields, IEEE Transactions on Visualization and Computer Graphics, 17(6):781–794, 2011.
[30] M. M. Malik, C. Heinzl, and M. E. Gröller, Comparative visualization for parameter studies of dataset series, IEEE Transaction on Visualization and Computer Graphics, 16(5):829–840, Sept. 2010.
[31] J. Schmidt, M. E. Gr¨oller, and S. Bruckner, Vaico: Visual analysis for image comparison, IEEE Transactions on Visualization and Computer Graphics, 19(12):2090–2099, Dec. 2013.
[32] M. Hummel, H. Obermaier, C. Garth, and K. Joy, Comparative visual analysis of lagrangian transport in cfd ensembles, IEEE Transactions on Visualization and Computer Graphics, 19(12):2743–2752, 2013.
[33] T. Peeters, P. Rodrigues, A. Vilanova, and B. Haar Romeny, Analysis of distance/similarity measures for diffusion tensor imaging. In D. Laidlaw and J. Weickert, editors, Visualization and Processing of Tensor Fields, Mathematics and Visualization, pages 113–136. Springer Berlin Heidelberg, 2009.
[34] S. G. Advani and C. L. Tucker, The Use of Tensors to Describe and Predict Fiber Orientation in Short Fiber Composites, Journal of Rheology, 31(8): 751–784, 1987.
[35]] N. Le. Behaviour law for the bmc composites, In IV European Conference on Computational Mechanics, page 3, 2010.
[36] D. Alexander, J. Gee, and R. Bajcsy, Similarity measures for matching diffusion tensor images, In Proceedings of the British Machine Vision Conference (BMVC), pages 93–102, 1999.
[37] W. Schroeder, K. Martin, and B. Lorensen. The Visualization Toolkit, Third Edition. Kitware Inc., 2004.
[38] C. Lorenz, I.-C. Carlsen, T. Buzug, C. Fassnacht, J. Weese, A multi-scale line filter with automatic scale selection based on the Hessian matrix for medical image segmentation, In Scale-Space Theory in Computer Vision, vol. 1252 of Lecture Notes in Computer Science, Springer Berlin Heidelberg, pages 152–163, 1997.
[39] M. Tessmann, S. Mohr, S. Gayetskyy, U. Hassler, R. Hanke, G. Greiner, Automatic determination of fiber-length distribution in composite material using 3d ct data, EURASIP J. Adv. Signal Process, 2010.
[40] O. Paetsch, D. Baum, K. Ehrig, D. Meinel, S. Prohaska, Automated 3D crack detection for analyzing damage processes in concrete with computed tomography, Conference on Industrial Computed Tomography, pages 321 – 330, 2012.
[41] F. Ihlenburg, Grundlagen der mathematischen Modellierung und numerischen Berechnung im Ingenieurwesen,2010.
[42] C. J. Taylor and D. J. Kriegman, Minimization on the lie group so(3) and related manifolds, Technical report, Yale University, 1994.
[43] J. Weissenböck, A. Amirkhanov, E. Gröller, J. Kastner, C. Heinzl, PorosityAnalyzer: Visual Analysis and Evaluation of Segmentation Pipelines to Determine the Porosity in Fiber-Reinforced Polymers, IEEE Conference on Visual Analytics Science and Technology, pages 101-110, 2016.
[44] A. Amirkhanov, A. Amirkhanov, D. Salaberger, J. Kastner, E. Gröller, C. Heinzl, Visual Analysis of Defects in Glass Fiber Reinforced Polymers for 4DCT Interrupted In situ Tests, Computer Graphics Forum, 35(3): 201-210, 2016.
[45] M. Sedlmair, C. Heinzl, S. Bruckner, H. Piringer, T. Möller, Visual parameter space analysis: A conceptual framework, IEEE Transactions on Visualization and Computer Graphics, 20(12): 2161-2170, 2014.
[46] C. Heinzl and S. Stappen, STAR: Visual Computing in Materials Science, Computer Graphics Forum, 36(3): 647-666, 2017.